

Article

Evaluation of Spatial Generalization Characteristics of a Robust Classifier as Applied to Coral Reef Habitats in Remote Islands of the Pacific Ocean

Justin J. Gapper ¹, Hesham El-Askary ^{2,3,4,*} , Erik Linstead ^{3,5}  and Thomas Piechota ³

¹ Computational and Data Sciences Graduate Program, Schmid College of Science and Technology, Chapman University, Orange, CA 92866, USA; gappe102@mail.chapman.edu

² Center of Excellence in Earth Systems Modeling & Observations, Chapman University, Orange, CA 92866, USA

³ Schmid College of Science and Technology, Chapman University, Orange, CA 92866, USA; linstead@chapman.edu (E.L.); piechota@chapman.edu (T.P.)

⁴ Department of Environmental Sciences, Faculty of Science, Alexandria University, Moharem Bek, Alexandria 21522, Egypt

⁵ Machine Learning and Assistive Technology Lab (MLAT), Chapman University, Orange, CA 92866, USA

* Correspondence: elaskary@chapman.edu; Tel.: +1-714-289-2053

Received: 3 October 2018; Accepted: 6 November 2018; Published: 9 November 2018



Abstract: This study was an evaluation of the spectral signature generalization properties of coral across four remote Pacific Ocean reefs. The sites under consideration have not been the subject of previous studies for coral classification using remote sensing data. Previous research regarding using remote sensing to identify reefs has been limited to in-situ assessment, with some researchers also performing temporal analysis of a selected area of interest. This study expanded the previous in-situ analyses by evaluating the ability of a basic predictor, Linear Discriminant Analysis (LDA), trained on Depth Invariant Indices calculated from the spectral signature of coral in one location to generalize to other locations, both within the same scene and in other scenes. Three Landsat 8 scenes were selected and masked for null, land, and obstructed pixels, and corrections for sun glint and atmospheric interference were applied. Depth Invariant Indices (DII) were then calculated according to the method of Lyzenga and an LDA classifier trained on ground truth data from a single scene. The resulting LDA classifier was then applied to other locations and the coral classification accuracy evaluated. When applied to ground truth data from the Palmyra Atoll location in scene path/row 065/056, the initial model achieved an accuracy of 80.3%. However, when applied to ground truth observations from another location within the scene, namely, Kingman Reef, it achieved an accuracy of 78.6%. The model was then applied to two additional scenes (Howland Island and Baker Island Atoll), which yielded an accuracy of 69.2% and 71.4%, respectively. Finally, the algorithm was retrained using data gathered from all four sites, which produced an overall accuracy of 74.1%.

Keywords: coral detection; classification; spectral signature expansion; benthic habitat mapping; Landsat 8

1. Introduction

Coral reefs are among the most complex and diverse ecosystems in the world [1]. However, these delicate ecosystems are under extreme threat due to numerous environmental and anthropogenic forces. Ocean acidification and mass bleaching events leading to large scale coral death is well documented [2–10]. Therefore, monitoring of these ecosystems is critical to inform policy and decision making for all agencies and at all levels. A comprehensive plan for evaluating the health of these

delicate ecosystems is a complex endeavor that can only be achieved through the combined efforts of both detailed in-situ analyses and efficient, large scale analyses.

Historically, studies of coral reefs have relied on manual surveys [11–15], which are prohibitively expensive to operate at scale [16]. More recently, remote sensing data has been used to evaluate individual sites. The most common sensors suitable for coral detection are SPOT High-Resolution Visible (HRV), Landsat Multispectral Scanner (MSS), Thematic Mapper (TM), Enhanced Thematic Mapper Plus (ETM+), Operational Land Imager (OLI), IKONOS, Advanced Airborne Hyperspectral Imaging System (AAHIS), Airborne Visible/Infrared Imaging Spectrometer (AVIRIS), and Sentinel-2 [17–25]. However, it is noteworthy that there are many more satellites available that can provide remote sensing data for coral reef analysis [26–28]. The 400 nm–600 nm wavelength spectral radiance is known to be useful in the mapping of ocean habitats including coral [29–31]. This visible light portion of the spectrum can penetrate ~15 to 30 m through clear waters, depending on turbidity and water quality [32]. Therefore, remote sensing data in these bands can contain information regarding the presence of coral on the ocean floor. Yet, this penetration depth is wavelength dependent as it decreases with longer wavelengths [33]. As a result, the blue spectral bands (400 nm) attenuate more slowly than red spectral bands (600 nm) [34]. This is particularly important because coral detection does not only come with spatial and spectral limitations, but also the confounding influence of variable depth on bottom reflectance, and disturbances due to turbidity of the water column [35–38]. These factors significantly influence the spectral reflectance of coral causing the signal received by the sensor to be highly dependent on the depth of the marine environment [39,40]. Therefore, water column and atmospheric corrections are needed in addition to adjusting for sun glint to accurately detect the existence of coral within a pixel [41–43]. Coral environments are among the most diverse environments in the world, and therefore, the spectral radiance can have some degree of variation even within a single pixel as the coral species varies within the location. In addition, coral environments are often heterogeneous, exhibiting a complex mixture of bottom types within a single pixel. This poses further challenges when using remote sensing data to detect coral's characteristics, such as the diversity and cover of coral species within each pixel according to the resolution available from a given spectrometer. These factors weaken the ability of a classifier to accurately determine the existence of coral. This is because satellites equipped with lower resolution spectrometers will tend to capture more heterogeneity within each pixel, and in turn deliver more mixed information regarding spectral reflectance to the classifier.

There have been a multitude of studies that leverage remote sensing data to evaluate reef health on an in-situ basis. These studies isolate a single location and provide in depth analysis of reef health for that site. Many such studies are temporal, also called spectral signature generalization and expansion [44] and therefore provide invaluable insight into the impact of climate change and the resulting site-specific environmental transformation. While these studies consistently reiterate the spectral signature generalization properties as they relate to a single site temporally, they do not address the spatial generalization properties of the spectral signature across multiple sites. If the existing in-situ studies are considered temporal studies, the progression based on spatial generalization can be considered a longitudinal or spatial study. While temporal studies have been conducted to evaluate the generalization properties of remote sensing information across seasons and years, evaluation of the spectral signature generalization properties across various proximities will measure the larger impact of disparate environmental conditions spatially, in addition to variations in the spectral reflectance of the coral ecosystems themselves. This longitudinal analysis will account for any location-based bias that previous in-situ analysis could not account for. Studying this bias and how well information contained within spectral reflectance generalizes spatially, in combination with the existing knowledge of how well spectral reflectance generalizes temporally, will significantly enhance our scientific understanding of detecting coral using remote sensing data. Furthermore, this knowledge will augment the existing research to enable temporal analysis on a larger scale than previous in-situ efforts. This research has been conducted with these far-reaching goals in mind. Specifically, we have focused on Landsat data, since there is a rich anthology of historical scenes which can be analyzed. We have limited our usage

of the existing Landsat bands only to those which have been available historically and not the coastal aerosol band, which is only available on the most recent Landsat 8 mission.

In this study, we evaluated the spatial generalization principles of the spectral signature across sites and scenes when applied to the detection of coral reefs. We considered four different locations across three different Landsat 8 scenes where coral reefs are known to exist. Our implementation accounts for obstructions in the image (clouds, shadows, dropped pixels, etc.), applies a water mask, corrects for atmospheric obstructions and sun glint, then calculates depth invariant indices across the image. Using the corrected depth invariant outputs of these preprocessing steps, we then applied linear discriminant analysis (LDA) to predict the presence of coral. After evaluating the accuracy of this in-situ analysis, we trained an LDA algorithm for application to coral cover type in another location within the same scene. Finally, we applied the linear discriminant analysis function to several sites in different Landsat scenes and analyzed the results. The methodology is a representation of the common data and applied science practice of splitting a dataset into training and testing sets. Many in-situ, temporal analyses perform train and test splits when creating a classifier, as it is the most appropriate thing to do; however, there is an inherent bias between train and test samples of a single site simply due to the common environmental factors influencing the model input features. This bias is more pronounced when samples are in close proximity to each other. The result is a model that is trained and assessed using only localized observations from a single site and therefore will not generalize well longitudinally. The reason is those observations do not adequately represent observations from other locations due to fluctuations in environmental conditions, including water turbidity, the diversity of marine life, and the bottom cover type itself, as well as unique geomorphological features that may be specific to a single location. Training a model on a given site and then evaluating performance on another site will eliminate this localized bias. As the distance between training and testing observations increases, the influence of environmental factors on both the train and test data from that unique site is reduced or eliminated. The result is a novel model that is trained on a diversity of environments and conditions enabling the output to be more robust than in-situ analysis to location bias, and therefore generalize more effectively.

In this paper, the first section will discuss the materials and methods used in the study, including a description of the data used and the geomorphology of each site, as well as the steps taken to preprocess the satellite images. The Materials and Methods section is followed by a review of the per site results, a quantitative assessment of the site-specific generalization performance and an evaluation of a robust model constructed using consolidated information from all the sites. The Discussion section of the paper includes an examination of the spectral signature generalization properties as it pertains to coral reef detection, an appraisal of the benefits and challenges of the methods evaluated in the research, followed by a proposal for future work in the area. The paper closes with a discussion regarding conclusions and outcomes resulting from this research.

2. Materials and Methods

2.1. Data Used

Images from Landsat-8 OLI with 30-m spatial resolution were used in the analysis. The visible bands were used due to their water column penetration properties, with band 2 corresponding to 0.450–0.515 μm (blue), band 3 corresponding to 0.525–0.600 μm (green), and band 4 corresponding to 0.630–0.680 μm (red). Band 5, which represented near infrared (NIR), was used to identify areas of full wavelength absorption for water masking. For each location of the analysis, Landsat 8 images produced within 6 months of the ground truth observation date were used [45,46]. Scenes were restricted to no more than 10% cloud cover and the remaining images were then inspected to determine which were most appropriate, including factoring in the location of clouds and other disturbances in the observation areas. In total, three different scenes were selected in the Pacific Ocean for our experiment as shown in Figure 1. A listing of each site and the associated Landsat scene Row-Path reference is

provided in Table 1. It is noteworthy that the first two sites were within the same path/row scene, hence the three scenes here are representing four sites.

Table 1. Selected Scenes for Study.

Location (Figure 1)	Path/Row	Location	Image Capture Date	Area of Interest Size	Number of Observations	Distance from Observation Site (Palmyra Atoll)
1	065/056	Palmyra Atoll (1)	27 May 2015	19 × 5-km	82	–
2	065/056	Kingman Reef (1)	27 May 2015	16 × 8-km	57	67.9-km
3	060/073	Baker Island Atoll (2)	20 August 2014	9 × 11-km	26	1709.6-km
4	059/074	Howland Island (4)	18 January 2015	9 × 8-km	30	1719.6-km

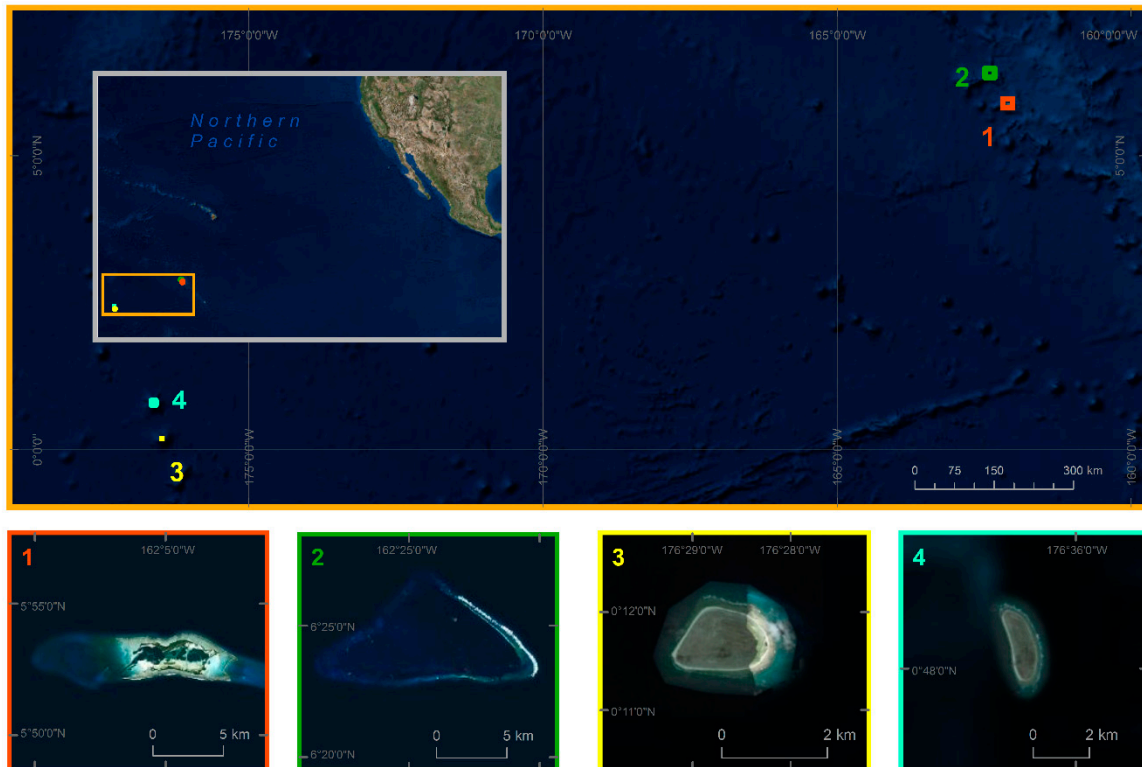


Figure 1. The location of the four sites (1) Palmyra Atoll, (2) Kingman Reef, (3) Baker Island Atoll, and (4) Howland Island.

2.2. Sites

2.2.1. Palmyra Atoll

Palmyra Atoll is a 20-km long elliptical reef located at 5°52'N 162°6'W within the Northern Line Island chain. It contains elongated terraces that extend 3 to 5 km off both the east and west ends of the atoll, the depths of which range from 7 to 25 m [47]. Benthic environments in the backreef are generally characterized by high rugosity, continuous reefs consisting of >50% live coral, interspersed with large, dead, standing corals [48]. Benthic fore reef habitats are dominated by hard coral and crustose coralline algae, together comprising 48% of all surfaces [49]. Halimeda and turf algae dominate fore reef benthic algal assemblages [50]. The lagoon is heavily degraded, characterized by high turbidity, sedimentation, and a benthos dominated by sponges with very few corals observed [51]. Coral reefs are concentrated on the westward reef terrace with algae accumulation primarily along the reef crest and within the lagoon. Over 50% of the hard coral at the site is comprised of *Montipora*, *Porites*, *Pocillopora*, and *Pavona* genera [52]. The isolated area of interest containing the Palmyra atoll with masked land and cloud pixels is shown in Figure 1.

2.2.2. Kingman Reef

Kingman Reef is the northern-most reef in the Line Island chain located 68 km northwest of the Palmyra Atoll at $6^{\circ}23'N$ $162^{\circ}25'W$. The atoll is triangular, stretching 18 km east-west and 9 km north-south [53] with shallow (<2 m) reefs along the southern and northern sides that are connected by a deeper reef (>20 m) along the western terrace. The atoll contains 2 small rubble islands near the eastern ends of the shallow reefs but lacks permanent emergent land. The lagoon is predominantly deep (>30 m) with large patch reefs that range from 50 to 200 m in diameter and extend to within 2 to 10 m of the surface. The lagoon side of the reef crest is comprised of a steeply sloped back reef habitat. The fore reef is consistent along the northern and southern coasts originating with a gradually sloped terrace extending 30 to 60 m from the reef crest with a drop-off beginning at ~20 m deep [54]. The most commonly occurring hard coral genera within Kingman Reef are *Porites*, *Pocillopora*, *Acropora*, and *Favia* which comprise >50% of all hard coral cover at the location [52]. Figure 1 exhibits the Kingman Reef area of interest with masked cloud cover. In addition, a small portion of exposed rubble can be observed on the eastern portion of the northern reef crest.

2.2.3. Baker Island Atoll

Baker is an outlier island of the Phoenix Island Archipelago and classified as a low reef island. The shallow marine benthic habitats consist of fringing reef crests, shallow back reefs, steep fore reefs, spurs-and-grooves, and small reef terraces. The west, north, and south of the island consists of steep reef slopes that descend to great depths [55]. The easterly side of the island is characterized by spurs-and-grooves and oligotrophic waters off reef terraces [56]. However, the island's proximity to the equator ($0^{\circ}12'N$ $176^{\circ}29'W$) causes it to be influenced by both the westward-flowing Southern Equatorial Current at the surface and the strong eastward-flowing Equatorial Undercurrent, resulting in nutrient rich topographic upwelling on the western side of the island [57]. *Acropora* comprise >60% of coral observed at the location while *Fungia* and *Pocillopora* are also common genera [57]. Figure 1 includes a display of the Baker Island Atoll area of interest with land and cloud mask applied.

2.2.4. Howland Island

Howland Island is located at $0^{\circ}48'N$ $176^{\circ}37'W$, just 66 km northwest of Baker Island; however, they fall in two different Landsat 8 scenes. As a result, they share many common environmental features, but the two sites are captured in separate path-row images. Similar to Baker Island, Howland Island is also classified as a low reef island and considered an outlier island of the Phoenix Island Archipelago. The Island's geomorphology consists of a narrow, shallow fringing reef and a steep slope that descends to great depths just off the coast. The western coast of the island is sandy and low while the waves and trade winds have caused the eastern side to be more abrupt and covered with coral rubble [58]. Given the island's proximity to the equator, it also is impacted by topographic upwelling of rich nutrients as the Southern Equatorial Current and Equatorial Undercurrent encounter the abrupt west slope of the island [57]. However, the hard coral species that exist in the habitat are somewhat different from what can be observed at Baker Island. The most abundant genera are *Pocillopora*, *Pavona*, *Porites*, *Montipora*, and *Fungia*, which is more similar to the representation found at Palmyra Atoll [57]. Figure 1 includes a presentation of the Howland Island area of interest isolated for study and processing, with a land and cloud mask applied.

2.3. Methodology

The overall layout of the processing approach applied to the three selected scenes is shown in Figure 2. The approach can be broken down into six major components: Preprocessing the image for land, water, and cloud masking, atmospheric and water column correction, LDA model training, LDA model application, model performance evaluation, and analysis of model generalization properties. These steps were repeated for each of the four sites within the three scenes. Scenes were

selected to minimize the presence of clouds in the image. Pixels that still suffer cloud cover or other obstructions were then identified and masked. This is followed by creating a water mask by applying a threshold to the near-infrared (NIR) band. The optimal threshold to use for the water mask is beyond the scope of this paper; however, a clustering method such as k-means with two classes can be employed across the area of interest to identify pixels with full wavelength absorption and pixels without full wavelength absorption. The reflectance cutoffs employed for each scene in this study ranged from 0.31 to 0.325. The water body and corals have similar spectral reflectance, which may lead to misclassification in water/coral areas. A deep-water area of interest (AOI) was selected to be used in atmospheric correction via the dark-pixel subtraction method [30,59,60]. An LDA application was then implemented and trained on the Palmyra Atoll site data. LDA is a frequently applied algorithm in studies involving classification based on remote sensing data. The algorithm attempts to discriminate discrete classes using a linear combination of continuous independent variables. In this way, the algorithm characterizes coral pixels based on a pooled covariance matrix of the pixel values and prior probabilities of the classification groups. A decision boundary between the classes is determined and observations are assigned to the class from which it has the smallest squared deviance [61,62]. Accuracy of the algorithm was evaluated using a leave one out cross validation. The model trained using Palmyra Atoll site observations was then applied to Kingman Reef site data (also within Path/Row 065/056) and the resulting performance was evaluated. Finally, the same model was applied to sites in several different scenes namely Baker Island Atoll and Howland Island. The resulting model performance was measured and analyzed, and its implementation was created using the open source R programming language and environment for statistical computing [63].

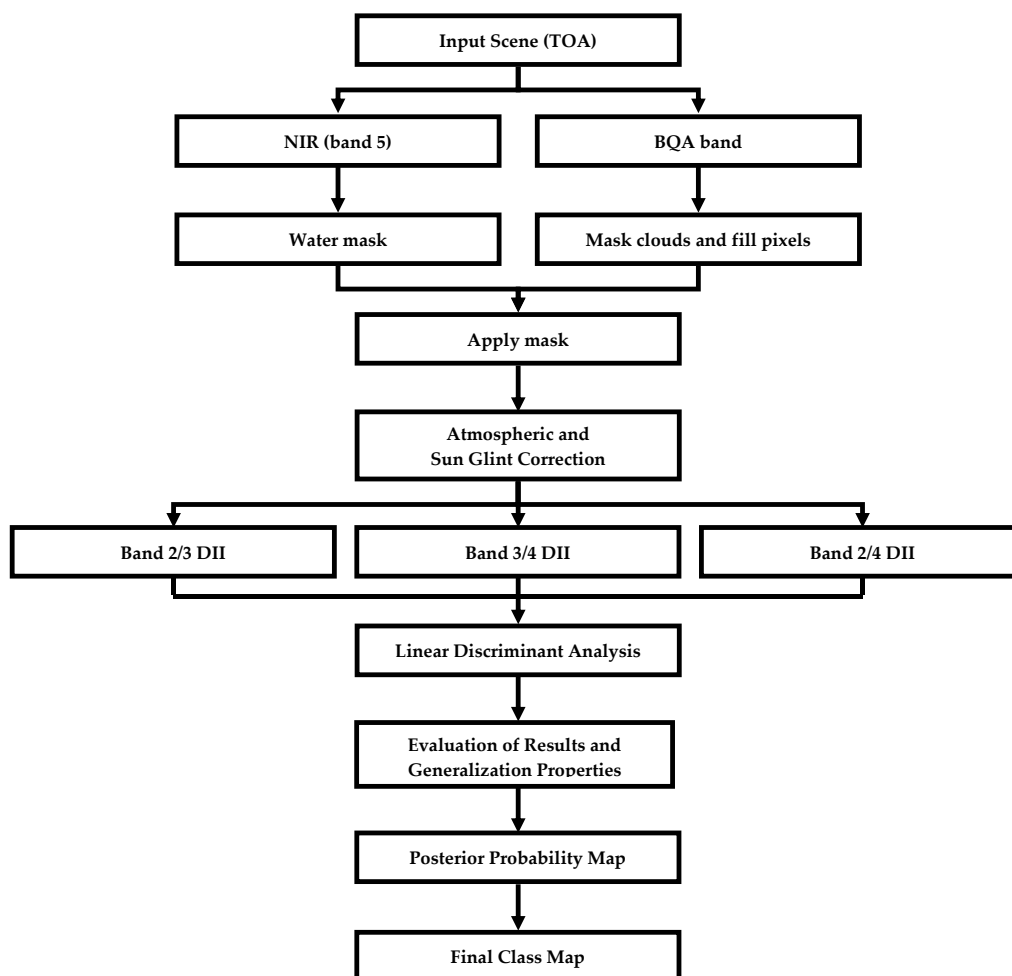


Figure 2. Scene masking, atmospheric correction, and water column correction process flow.

2.3.1. Cloud and Quality Mask

The first step taken to preprocess the selected images was the identification and masking of pixels obscured by cloud cover and shadows. While scenes were selected to minimize the amount of cloud cover, none of the images were completely devoid of clouds. Given the location of the sites, the Pacific Ocean near the equator, and the six-month window constraint, the probability that a satellite image would be taken on a cloud free day is small. Masking of clouds was performed by leveraging the Landsat 8 product quality band [64], which provides a per pixel approximation of confidence that a given condition exists [65]. There are several possible ways in which bias from cloud obstruction can contaminate an analysis. The obvious entry point is disrupting the reflectance of a pixel or group of pixels. In addition to directly influencing surface reflectance, cloud cover present in the deep-water AOI can alter the values used for atmospheric correction applied to the image through the dark-pixel subtraction method [66]. As a result, this initial step of masking cloud interference was a critical preprocessing step.

2.3.2. Water Mask

The study of DII related metrics across large scenes requires preprocessing that includes masking land in addition to clouds and shadows. This step is imperative as including land pixels can distort the DII parameters when calculated across a scene. The water mask was created by leveraging the Landsat 8 NIR sensor. This sensor measures light between 0.851 and 0.879 μm . Water absorbs light in these wavelengths therefore, it is a good candidate for discerning water from land in any given scene [67]. As in the visible bands, the Landsat 8 NIR band (band 5) is at a 30 m resolution. A threshold was applied to the NIR band pixel values of each scene. The plots were then evaluated visually to determine the most appropriate cutoff for separation of land and water. A mask was created for pixels determined to be water based on this threshold value.

2.3.3. Atmospheric Correction

In the visual bands, 90% of the at sensor reflectance depends on atmospheric and water surface properties [68]. Therefore, atmospheric correction is first performed using the dark pixel subtraction method [69]. This method selects areas of the scene with water known to be deep enough for the visible bands to fully attenuate. Signals received from these areas are comprised of atmospheric radiance and surface reflectance, thereby isolating the impact of these elements. Assuming the atmospheric and water surface conditions generalize to the rest of the scene (i.e., uniform throughout the area of interest), the mean deep-water radiance at sensor can be leveraged to correct for the effect of atmospheric and surface reflectance interferences [34,70,71]. Depths greater than 50 m will assure that the visible wavelengths have fully attenuated [72]. In addition, two standard deviations are subtracted to account for possible sensor noise [73]. It is important to highlight the assumption that conditions are uniform across each scene. In addition, because of this assumption, the deep-water AOI selected should appear in the same scene that is being analyzed. This will minimize the possibility of unintended bias that may be introduced by leveraging a deep-water AOI of another image and that to the greatest extent possible, the effect of full attenuation of the wavelengths for each scene is uniquely isolated.

2.3.4. Water Column Correction

As light penetrates water, the intensity decreases exponentially with increasing depth. The rate of attenuation is wavelength-dependent and has a severe effect on the remote sensing-based detection of aquatic habitats [34]. Therefore, water column correction is appropriate for imagery with multiple water-penetrating spectral bands [60,74]. Within these visible spectral bands, longer-wavelength blue bands attenuate less rapidly than shorter-wavelength red bands. Therefore, the spectral radiances recorded at sensor are dependent on both the subsurface strata reflectance and depth. The confounding influence of depth can create significant distortions in the subsurface reflectance. Since most marine

habitat-mapping exercises are only concerned with mapping benthic features, it is advantageous to remove the influence of variable depth [34,74–77].

3. Results

Using the masked, corrected scenes, we developed a classifier to identify the existence of coral in a pixel. We applied the predictor to an alternate site within the same Landsat scene (Kingman Reef). Finally, we applied the predictor to multiple sites in different Landsat scenes (Baker Island Atoll and Howland Island).

3.1. Generalization Performance by Site

3.1.1. Palmyra Atoll

The model was initially trained and applied to data from the Palmyra Atoll site of Landsat Path-Row scene 065/056. This site contained a total of 82 unique observation points. Of these, 66 were in unobscured pixels. For each valid observation point, the corresponding pixel index values were extracted from the masked, atmospherically corrected, and water column corrected scene based on location. The extracted DII values were then matched to the ground truth class. The LDA model was trained on these observations.

For each pixel, the posterior probability of that pixel belonging to the coral class was calculated. This posterior probability for each pixel belonging to the coral class is shown in Figure 3. The resulting map of predicted values was analyzed and compared to known geomorphology of the site for context validation. Figure 4 displays the final class predictions by pixel, based on the trained model.

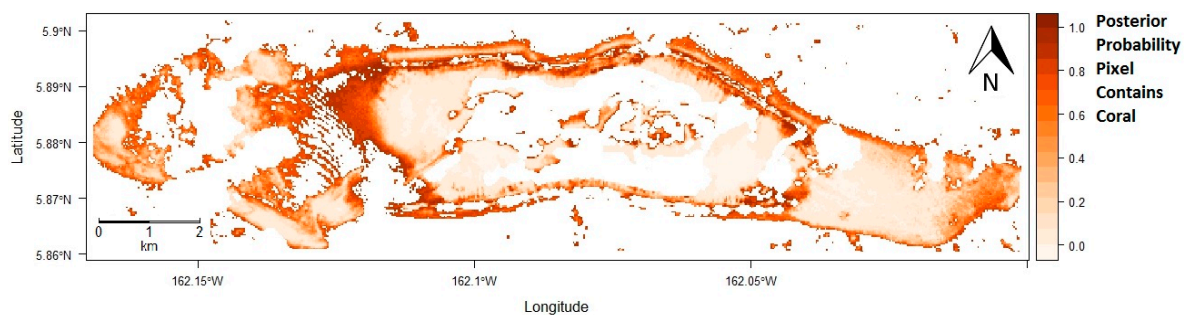


Figure 3. Palmyra Atoll: Plot of the posterior probability for belonging to the coral class for each pixel in the Palmyra Atoll site.

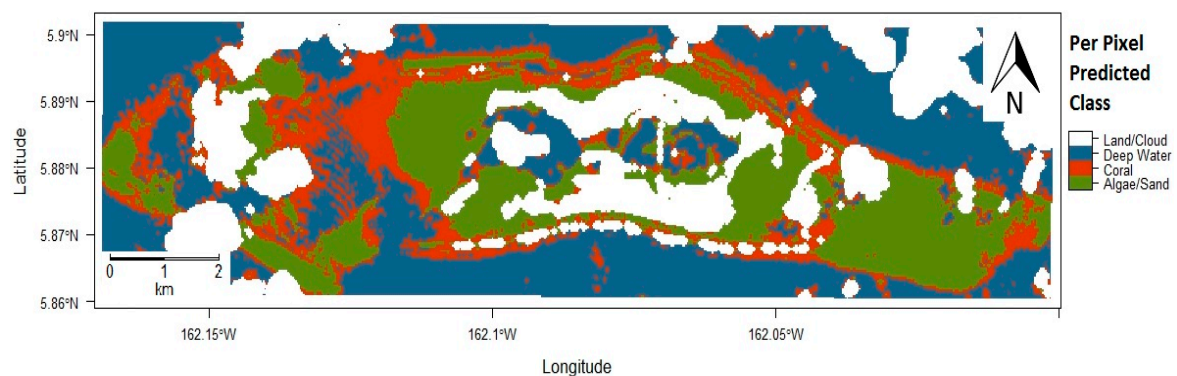


Figure 4. Palmyra Atoll predicted class membership based on posterior probabilities.

3.1.2. Kingman Reef

The first evaluation of how well a supervised classifier can generalize across multiple sites was evaluated by applying the model trained on the Palmyra site data to labeled data from another location within the same Landsat scene. This was done by predicting labeled data from the Kingman Reef using the algorithm trained on data from the Palmyra Atoll. The Kingman Reef is a small reef near Palmyra Atoll, therefore the two locations reside within the same Landsat image. Sites within the same scene will have similar atmospheric and water conditions, an assumption that previous in-situ studies have relied upon heavily. Water turbidity, in particular, is an important assumption as water column correction has yet to produce a proven method for correcting such interferences or even evaluating its impact on predicting subsurface benthic habitat bottom type.

There were 57 bottom type observations available for the Kingman Reef site. Of these, 42 could be matched to valid pixels in the masked, atmospherically corrected, and water column corrected scene. The trained model correctly predicted 78.57% of the observations in the Kingman Reef site. This is evidence that the model built using water column corrected indexes generalizes well to sites within the same scene. The decrease in accuracy from Palmyra Atoll to Kingman Reef of less than 1% is strong evidence for the within scene homogeneity assumption relied on so heavily in previous in-situ studies. The strong performance reflects the location based environmental conditions that the two sites have in common. Specifically, because the two sites are within close proximity, they share similar atmospheric and geomorphological conditions. In addition, the marine species are likely to be more homogeneous compared to sites separated by a greater distance. Finally, water conditions at each site are likely to be similar but not identical. Site specific variation in water conditions can occur within a scene due to differences in how tides, currents, and other natural phenomena interact with site-specific geomorphological characteristics. The results indicated that the consolidated impact of all these factors amounts to less than 2% decrease in the accuracy of predicting bottom type between two sites within the same Landsat image. The resulting posterior probability that a given pixel belongs to the coral class are presented in Figure 5, and the overall class predictions are presented in Figure 6.

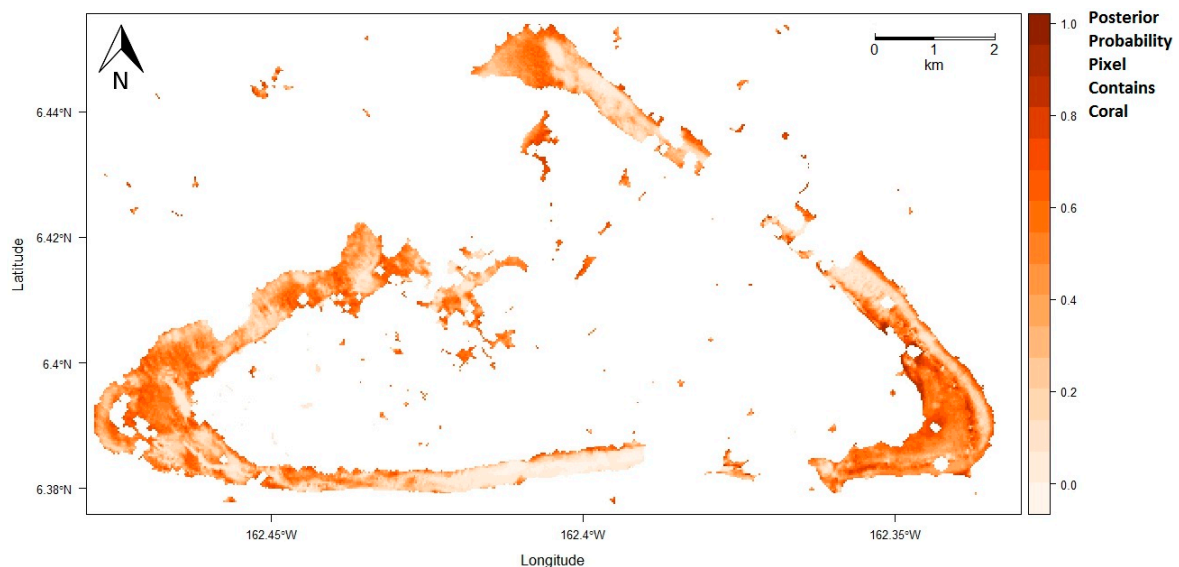


Figure 5. Kingman Reef: Plot of the posterior probability for belonging to the coral class for each pixel.

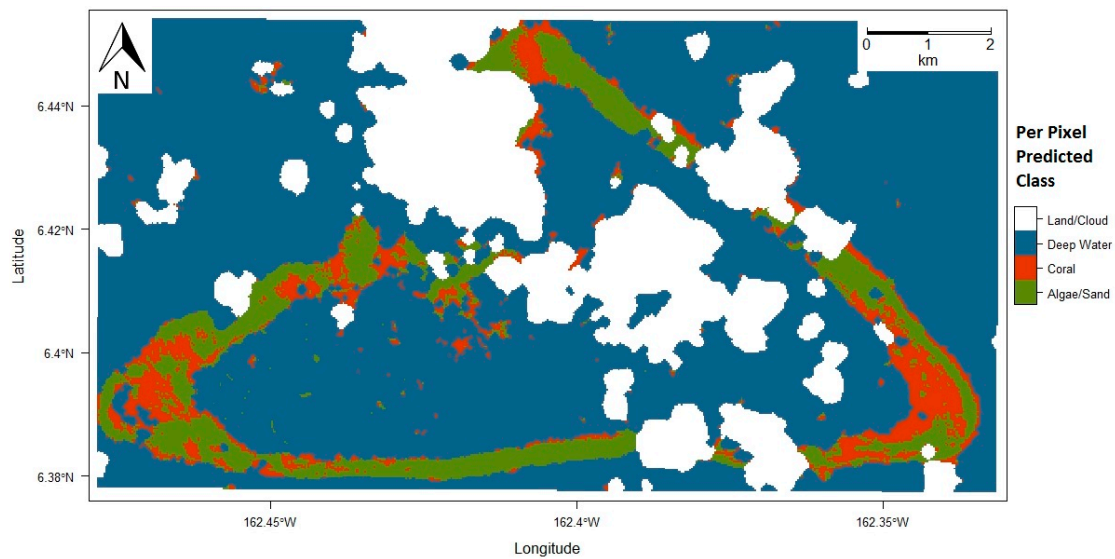


Figure 6. Kingman Reef predicted class membership based on posterior probabilities.

3.1.3. Baker Island Atoll

The ability of the classifier to generalize to a different scene is an important result. The conditions between scenes can change significantly. In addition, the variation of marine life species represented in different sites can alter the observed DII pixel value. Even more importantly, there are likely to be variances in how reefs naturally formed due to alterations in the site-specific geomorphology. Even with a uniform approach to atmospheric and water column correction, the environmental changes across scenes can be substantial.

The ground truth data from the Baker Island Atoll location included 26 bottom type observations all of which were associated with valid DII pixel values. The classifier trained on Palmyra Atoll data was able to correctly classify 69.23% of these observations. The decrease in accuracy can be attributed to changes in site-specific conditions between Baker Island Atoll and Palmyra Atoll. Differences in how currents and tides impact water turbidity, as well as other environmental impacts, reduce the ability for observations to appropriately represent other locations. Previous in-situ studies have relied on the assumption of uniform water conditions. This is because, while there may be significant obstruction of light due to matter floating in the water, it is not likely to be substantially different across a single scene. Therefore, because all observations are distorted by approximately the same amount, it only represents a uniform amount of noise across all pixels in a given scene. However, when data from one scene is used to evaluate a different scene, these changes in localized or image specific conditions become more pronounced. For example, changes in water conditions including turbidity can vary within a scene but is likely to be more similar between two sites within a scene compared to two sites located in separate images altogether. First, scenes in two separate images are likely to be separated by greater distance than those in the same scene. This gives rise to greater environmental fluctuation between sites that are separated by enough distance to be in two separate Landsat images. There are multiple similar reasons for this fluctuation in water conditions. Namely, the impact of currents and tides can vary from site to site. The unique location of Baker Island Atoll relative to the equator compared to Palmyra Atoll and Kingman Reef expose it to more topographic upwelling of nutrient rich waters, which in turn impact the type of coral at the site and hinder the generalization of the trained model. In addition, the images of two different scenes were captured on different times and dates that likely had varying weather and ocean conditions. The consolidated impact of variation on accuracy due to the limited observations and to generalizing beyond the in-situ image is now measured. For example, the total impact of site specific environmental conditions between Palmyra Atoll and Baker Island Atoll represents an 11% decrease in accuracy between the two sites. The resulting per pixel posterior probabilities for the bottom type to be coral and the per pixel predicted class are presented in Figures 7 and 8, respectively.

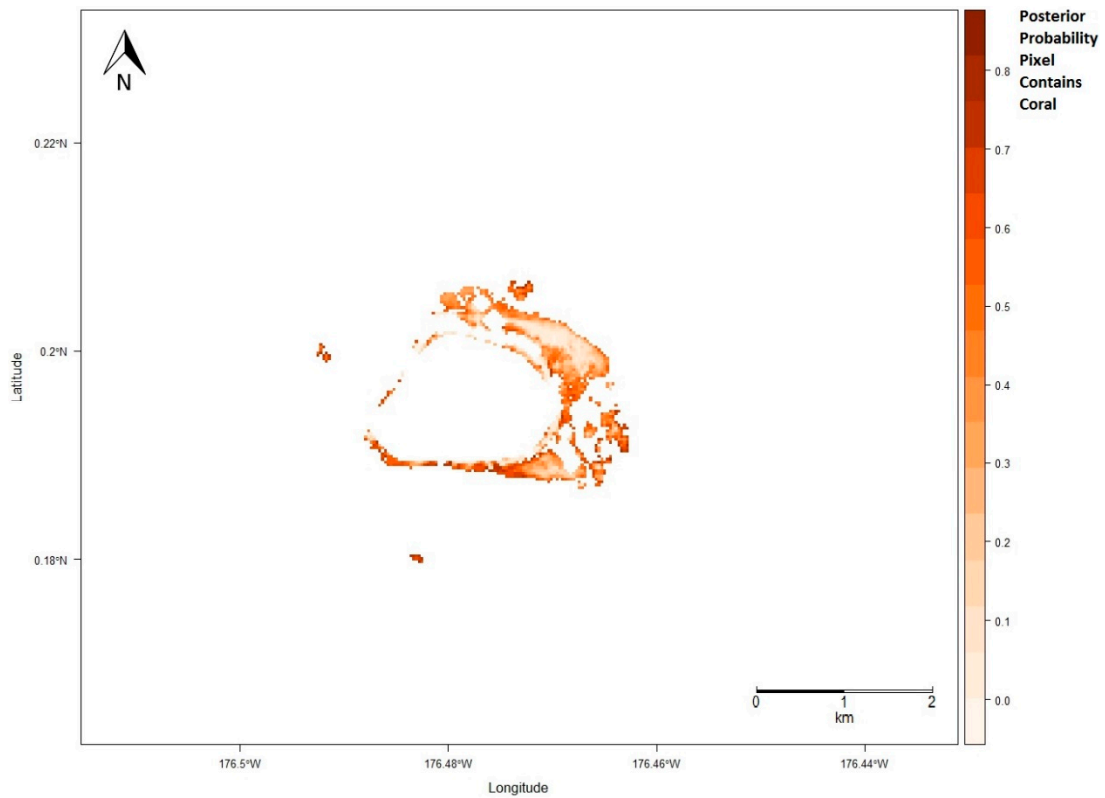


Figure 7. Baker Island Atoll: Plot of the posterior probability for belonging to the coral class for each pixel in the Baker Island Atoll site.

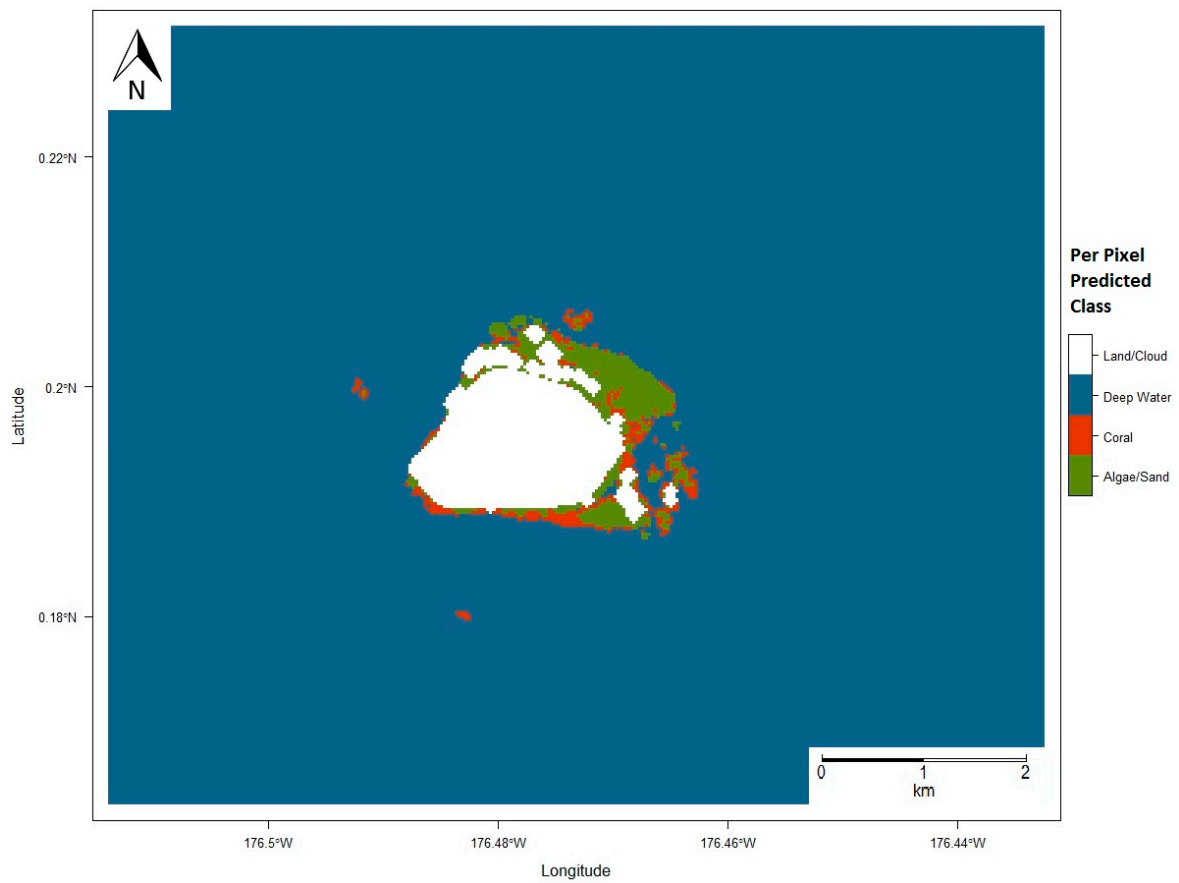


Figure 8. Baker Island Atoll predicted class membership based on posterior probabilities.

3.1.4. Howland Island

Given the proximity and geomorphologic similarities between Howland Island and Baker Island, it can be assumed that the environmental conditions that exist within the two sites are similar relative to some of the other locations. Therefore, the accuracies produced when the Palmyra Atoll model was applied to each site are similar but not identical. This result is informative in isolating the impact on generalization due to environmental variation associated with location versus the impact on generalization due to the timing in which the Landsat image was captured. There were 30 observations of bottom type at the Howland Island site of which 28 could be assigned valid depth invariant pixel values. When applied to the Howland Island site, the model correctly predicted 71.43% of the observations.

Figure 9 presents the per pixel posterior probability that the pixel contains coral. Since the two sites are not close enough to reside within the same Landsat scene, they do not get the benefit of uniform interference across the scenes. The result is accuracy scores that are comparable due to environmental and species similarities within the two sites, but not identical. The consolidated effect of these variations in conditions between the Palmyra Atoll training data and Howland Island test site was an 8.87% decrease in accuracy of bottom type prediction between the two sites. Figure 10 presents the final class predictions for each pixel in the Howland Island area of interest.

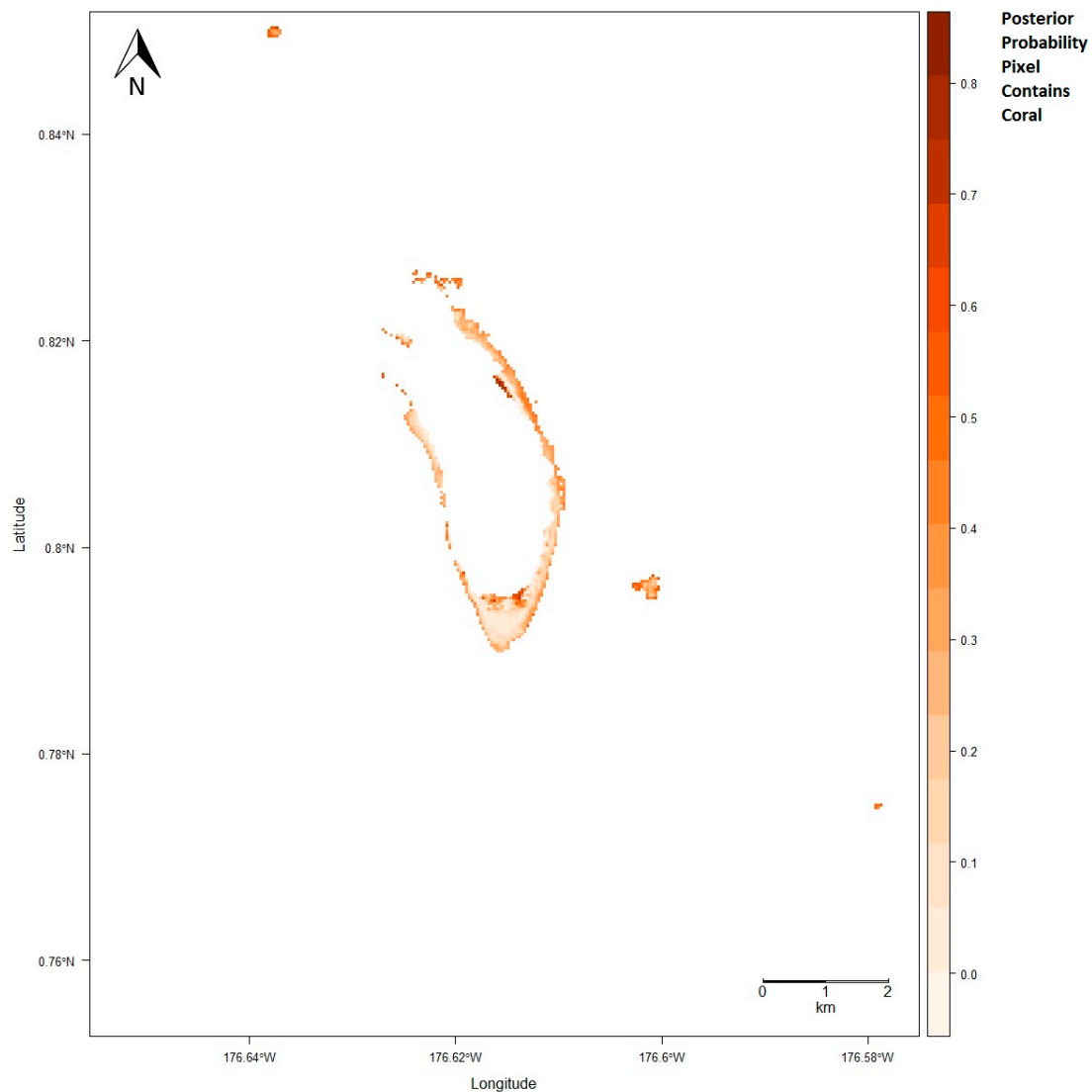


Figure 9. Howland Island: Plot of the posterior probability for belonging to the coral class for each pixel in the Howland Island site.

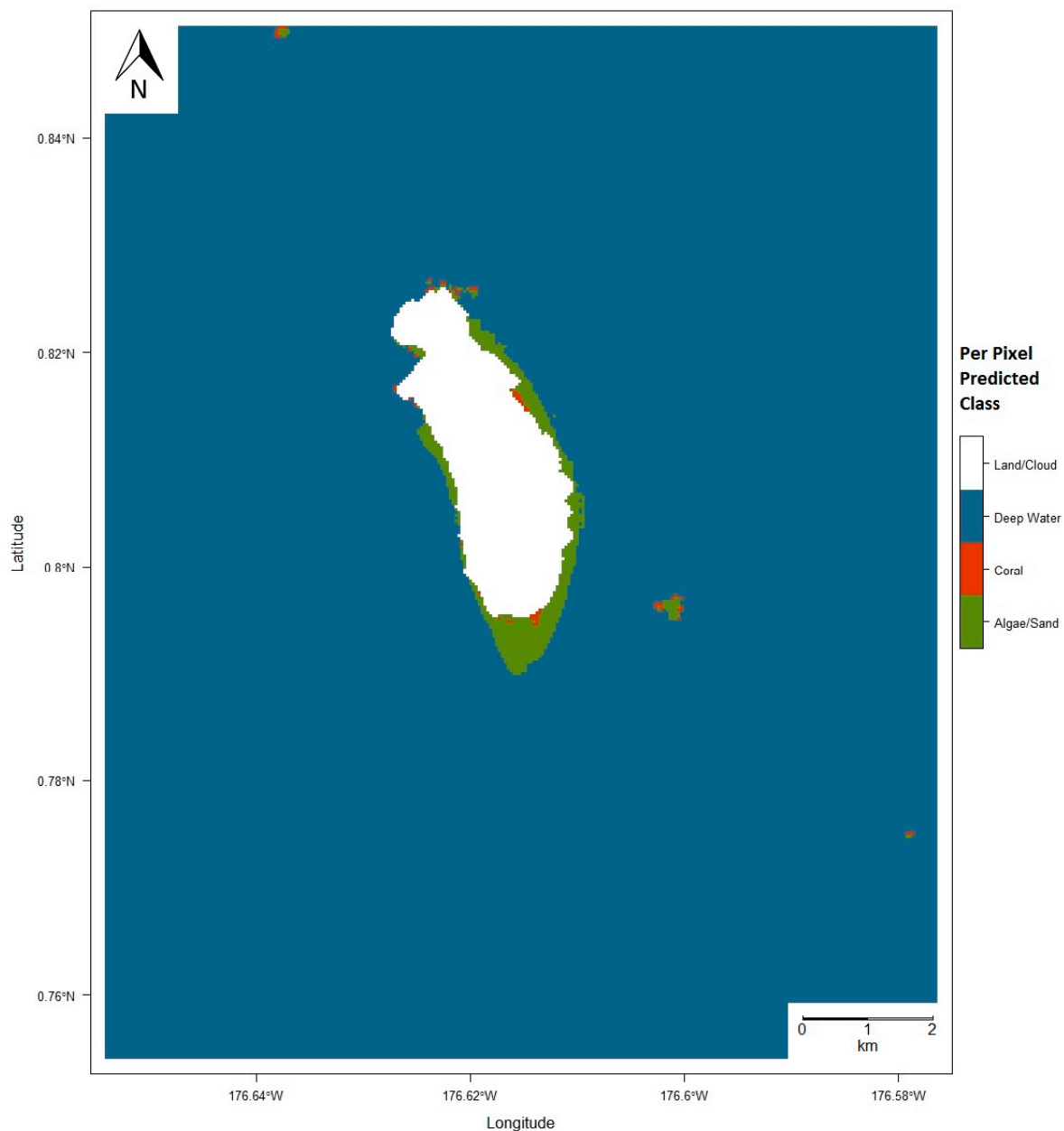


Figure 10. Howland Island predicted class membership based on posterior probabilities.

3.2. Quantitative Assessment of Site Specific Generalization

The algorithm correctly classified 80.30% of the observations within the Palmyra Atoll site and obtained a precision of 0.7800 and recall of 0.9512. Precision and recall are very common statistical measures for measuring type I and type II error rates. Precision is a measure of type I errors and commonly thought of as a measure of the exactness of an algorithm. Recall is a measure of type II errors and is often thought of as a measure of how completely the algorithm retrieves information. The harmonic mean of precision and recall is known as the F-measure. The results of the model application to the Palmyra Atoll site yielded an F-measure of 0.8571. Finally, specificity, which is an indication of the algorithm's ability to differentiate between true negative observations, was 0.5600 when evaluated against the Palmyra Atoll truth data.

When applied to the Kingman Reef site, the algorithm obtained similar performance to that observed in the Palmyra Atoll site. Specifically, the Kingman Reef application accurately classified 78.57% of the observations with precision and recall of 0.8276 and 0.8571, respectively. This indicates

that the model outperformed the original site in type I error when applied to the Kingman site, but committed more type II errors as well. The model obtained a specificity of 0.6429 and an overall F-measure of 0.8421, both of which are similar results to those obtained from the Palmyra site. The similarity between the two sites can be attributed to their close proximity and commonality in environmental conditions.

Evaluation of the model performance when applied to the Baker Island Atoll site revealed 69.23% of the ground truth observations could be correctly classified. Further evaluation of the algorithm results showed that the algorithm yielded precision and recall of 0.6522 and 1.0000, respectively. The F-measure for the application was 0.7895, which was similar to the measure produced in the evaluations of previous sites. Specificity equal to 0.2727 was obtained.

The Howland Island application produced more type II errors than observed in other scenes, and as a result, had a low recall score of 0.5333. Specificity scored higher than the applications to other sites with a score of 0.9231, due to fewer type I errors. Owing to the low type I error rate, precision was high at 0.8889. The F-measure was the lowest of all applications at 0.6667. These results are summarized in Table 2, followed by the detailed confusion matrices in Table 3.

Table 2. Assessment metrics for evaluation of model performance for each site and consolidated input.

	Palmyra Atoll	Kingman Reef	Baker Island Atoll	Howland Island	Consolidated Sites
Accuracy	80.30%	78.57%	69.23%	71.43%	74.07%
Precision	0.7800	0.8276	0.6522	0.8889	0.7244
Recall	0.9512	0.8571	1.0000	0.5333	0.9293
Specificity	0.5600	0.6429	0.2727	0.9231	0.4444
F-measure	0.8571	0.8421	0.7895	0.6667	0.8142

Table 3. Confusion Matrices by Site and Consolidated Inputs.

		Ground Truth Labels	
		Coral	Not Coral
Predicted Class	Palmyra Atoll		
	Coral	39	11
	Not Coral	2	14
	Kingman Reef		
	Coral	24	5
	Not Coral	4	9
	Baker Island Atoll		
	Coral	15	8
	Not Coral	0	3
	Howland Island		
Coral	8	1	
Not Coral	7	12	
Consolidated Sites			
Coral	92	35	
Not Coral	7	28	

3.3. Robust Combined Model

The accuracy for any given site is constrained by how well the observed values used to train an algorithm represent the general population, and how well the algorithm itself can correctly model the relationship between inputs and the target variable. One way to ensure that the observation data adequately represents the population is to increase the breadth of observations used to train the predictor. Having analyzed the variation in accuracy across the various sites, we retrained the model

using observations from all four sites. The resulting model was evaluated using a leave one out cross validation (LOOCV), for the classification of 127 coral pixels and 35 non-coral pixels. Of the 127 coral predictions, 92 were correct and 35 were incorrect. Of the 35 not-coral predictions, 28 were correct and 7 were incorrect, which corresponds to an accuracy of 74.07%. The classifier yielded a precision of 0.7244 and recall of 0.9293 indicating good performance on type II errors and marginal performance against type I errors. The model yielded a specificity of 0.4444 and the final F-measure was 0.8142.

These results expose the novel finding that a model can be trained on data from multiple Landsat sites and yield robust predictions of coral. The associated confusion matrix can be found in Table 3. The resulting model yielded strong results to data collected from multiple sites and multiple scenes. This is a demonstration of the robustness of Landsat data to generalize across scenes. However, the model did not obtain the same accuracy produced using data from a single scene or even the model applied to an alternate site within the same scene. This is due to the impact of variation in environmental conditions between scenes. Most notably, there are often significant differences in water conditions and turbidity across various locations. However, the impact of these differences can be mitigated as more sites are considered for training the model. In addition, there are variations in the marine species that exist across locations. These two factors confound the inputs for a predictive model and lead to lower accuracies. Previous research has relied on assumptions of homogeneity. Comparing the results of the Palmyra Atoll and Kingman Reef sites within the same scene confirms this assumption, although with a slight drop in accuracy. Figure 11 identifies the receiver operating characteristic (ROC) curve resulting from the model developed using the consolidated site data. This is an important visualization used to identify performance as a function of the type I error or recall (true positive rate) as a function of $1 - \text{Specificity}$ (false positive rate). The area under curve (AUC) is an important diagnostic for evaluating model performance related to the ROC curve. In this instance, the value of the AUC was 0.7298.

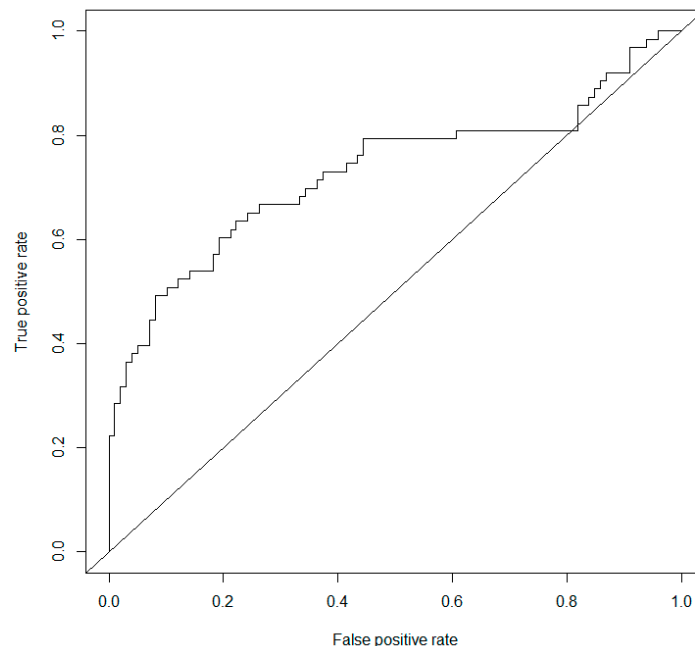


Figure 11. Receiver operating characteristic (ROC) Curve indicating model performance of the algorithm when applied to the consolidated ground truth set (Area under curve (AUC) = 0.7298).

4. Discussion

4.1. Spectral Signature Generalization Properties for Coral Reef Classification

The ability for a supervised classifier to generalize across sites is a critical outcome of this research. Previous research has concerned analysis and classifiers strictly limited to in-situ sites. This research

advances the field of subsurface identification by evaluating the ability for Landsat information to generalize across sites and scenes. We measured this by locating four different sites known to contain benthic areas with coral reefs. We then obtained corresponding ground truth labels for a sampling of coral and non-coral pixels for each location. A classifier was trained using linear discriminant analysis to predict the presence of coral. This model yielded a leave one out cross validation accuracy of 80.30% in the training site, and only a small decrease in accuracy when applied to a remote site within the same scene. The accuracy of the model when applied to the Kingman Reef site was 78.57% demonstrating that while conditions can change across a given scene, the impact was minimal. This validates the classic assumption made by previous in-situ studies of homogeneity of conditions across a given Landsat scene. We then applied the model to several other sites. Baker Island Atoll yielded an accuracy of 69.23%, and Howland Island produced an accuracy of 71.43%. These lower accuracies were due to two primary reasons. First, variances in the types of coral and algae species that live in a given ecosystem create small variations in the signal received by the satellite. This diversity of life is related to each ecosystem's adaptation to the surrounding geomorphic conditions. Changes in environmental conditions and related noise create disturbances that manipulate the signal received by the sensor. While atmospheric and light attenuation due to water column penetration can be corrected, the interference due to localized water turbidity cannot. This can account for a decrease in accuracy of predicting coral by more than 10%, as shown in this study. The interference due to water turbidity is not uniform and some scenes are impacted more than others. Finally, a consolidated model was created using the strength of observations across all sites. Accuracy of 74.07% was calculated using a leave one out cross validation. The resulting model demonstrated a robustness to some of the perturbations mentioned.

4.2. Methodology Benefits and Challenges

The outcomes presented in this study enabled a solution to reduce location-based bias of the spectral signature of coral reefs. This represents a strong advantage over previous in-situ studies, which required localized observation data to detect coral reefs. The results presented in this study indicated that the spectral signature information of coral contained in one site can be leveraged to evaluate another, unobserved site with up to 71% accuracy. Furthermore, the results of this study indicated that a robust model can be created by leveraging the consolidated information from several sites and produce accurate predictions for coral of up to 74%. These results are a key component required for the progression from in-situ analysis to large scale spatial analysis of coral reefs.

The primary challenge of the proposed method are the lower accuracy scores as compared to that of in-situ analysis. Previous in-situ analysis based on Landsat data generally obtain accuracies of up to 80% [37], as was obtained in the site-specific study of Palmyra Atoll here. The reduction in accuracy is an indication of variation in the geomorphology and ecology of the robust model. In-situ analyses incorporate this bias into the training of their predictors, and therefore yield higher accuracies.

4.3. Future Research

Future work is required to apply the spectral signature generalization principles of coral presented here. This research has intentionally adhered to two major restrictions to enable these future endeavors. First, we have focused on Landsat data, despite inferior resolution compared to newer satellites such as the Sentinel-2 mission. This was done so that analysis in the immediate future can build on the results presented here by leveraging temporal analysis of the rich history of Landsat missions. Beyond the immediate future, once a rich archive of Sentinel data is accumulated, this analysis can be leveraged to enable temporal analysis at higher resolutions. Similarly, we have omitted the use of the Landsat 8 Ultra Blue Band 1. While the wavelength penetration properties of this band would certainly add value to this analysis, we have avoided leveraging this information to enable change detection analysis that will rely on historical Landsat missions for which this band is unavailable. Future work is also

required to evaluate more sophisticated models such as support vector machines for pixel classification in multiple scenes and recurrent neural networks (RNN) for pixel change analysis and prediction [78].

5. Conclusions

The ability for a supervised classifier to generalize across sites is a critical outcome of this research. Previous research has concerned analysis and classifiers strictly limited to in-situ sites. This research advances the field of coral classification using remote sensing data by evaluating the ability for Landsat information to generalize across sites and scenes. This outcome is part of a natural progression toward a global evaluation of coral health using satellite data both in the present and historically. Understanding the spectral generalization properties of coral enables more robust evaluation of many reefs which have not been studied before. Furthermore, this research provides a baseline accuracy for evaluating the presence of coral in locations for which observations are unavailable or have not been made. The classification accuracy of the model trained on a known site and applied to a new site is less than that of previous in-situ analysis, because it does not incorporate the site-specific geomorphology and location-based bias. However, a model trained using data from multiple sites is more robust to these environmental variations and free of location specific bias. We measured the generalization criterion by locating four different sites known to contain benthic areas with coral reefs. We then obtained corresponding ground truth labels for a sampling of coral and non-coral pixels for each location. A classifier was trained using linear discriminant analysis to predict the presence of coral. This model yielded a leave one out cross validation accuracy of 80.30% in the training site and only a small decrease in accuracy when applied to a remote site within the same scene. The accuracy of the model when applied to the Kingman Reef site was 78.57%, demonstrating that while conditions can change across a given scene the impact is minimal. This validates the classic assumption made by previous in-situ studies of homogeneity of conditions across a given Landsat scene. We then applied the model to several other sites. Baker Island Atoll yielded an accuracy of 69.23%, and Howland Island produced an accuracy of 71.43%. These lower accuracies are due to two primary reasons. First, variances in the types of coral and algae species that live in a given ecosystem create small variations in the signal received by the satellite. This diversity of life is related to each ecosystems adaptation to the surrounding geomorphic conditions. Even more, changes in environmental conditions and related noise create disturbances that manipulate the signal received by the sensor. While atmospheric and light attenuation due to water column penetration can be corrected, the interference due to localized water turbidity cannot. As seen in this study, this can account for a decrease in accuracy of coral prediction by more than 10%. Furthermore, the interference due to water turbidity is not uniform and some scenes are impacted more than others. Finally, a consolidated model was created using the strength of observations across all sites. Accuracy of 74.07% was calculated using a leave one out cross validation. The resulting model demonstrated a robustness to some of the perturbations mentioned.

Author Contributions: J.J.G. implemented the methods, analyzed the data, and provided written sections to the corresponding author for revisions and inclusion. H.E.-A. led the research effort and came up with the idea and plan of work. He was involved in all steps of data rendering, analysis, manuscript writing, and revising. E.L. reviewed software source code, provided technical guidance with respect to the data analysis, and contributed to manuscript preparation. T.P. contributed valuable comments and helped with the logical flow of the entire manuscript. All authors read and approved the final manuscript.

Funding: This research received no external funding and the APC was funded by the MLAT lab.

Acknowledgments: The authors would like to thank Georgiana Bostean, Assistant Professor in the Department of Sociology and Environmental Science & Policy Program at Chapman University for her consultation as an expert cartographer. The authors would also like to acknowledge the use of the Samueli Laboratory in Computational Sciences in the Schmid College of Science and Technology, Chapman University, in data processing and analysis. Furthermore, the authors would like to acknowledge the support of Microsoft Corporation and Amgen Inc.

Conflicts of Interest: The authors declare no conflict of interest.

References

- Jessen, C.; Wild, C. Herbivory Effects on Benthic Algal Composition and Growth on a Coral Reef Flat in the Egyptian Red Sea. *Mar. Ecol. Prog. Ser.* **2013**, *476*, 9–21. [[CrossRef](#)]
- Aronson, R.B.; Precht, W.F. White-Band Disease and the Changing Face of Caribbean Coral Reefs. *Hydrobiologia* **2001**, *460*, 25–38. [[CrossRef](#)]
- Glynn, P.W. Coral Reef Bleaching: Ecological Perspectives. *Coral Reefs* **1993**, *12*, 1–17. [[CrossRef](#)]
- McManus, J.W.; Reyes, R.B., Jr.; Nañola, C.L., Jr. Effects of Some Destructive Fishing Methods on Coral Cover and Potential Rates of Recovery. *Environ. Manag.* **1997**, *21*, 69–78. [[CrossRef](#)]
- Pennisi, E. Survey confirms coral reefs are in peril. *Science* **2002**, *297*, 1622b–1623b. [[CrossRef](#)] [[PubMed](#)]
- Burke, L.; Reyntar, K.; Spalding, M.; Perry, A. *Reefs at Risk Revisited*; World Resources Institute: Washington, DC, USA, 2011; p. 114.
- Mora, C.A. A clear human footprint in the coral reefs of the Caribbean. *Proc. R. Soc. Lond. B Biol. Sci.* **2008**, *275*, 767–773. [[CrossRef](#)] [[PubMed](#)]
- Hoegh-Guldberg, O.; Mumby, J.P.; Hooten, J.A.; Steneck, S.R.; Greenfield, P.; Gomez, E. Coral reefs under rapid climate change and ocean acidification. *Science* **2007**, *281*, 1737–1742. [[CrossRef](#)] [[PubMed](#)]
- Pandolfi, J.M.; Bradbury, R.H.; Sala, E.; Hughes, T.P.; Bjorndal, K.A.; Cooke, R.G.; McArdle, D.; McClenachan, L.; Newman, M.J.H.; Paredes, G.; et al. Global trajectories of the long-term decline of coral reef ecosystems. *Science* **2003**, *201*, 955–958. [[CrossRef](#)] [[PubMed](#)]
- Hedley, J.C.; Roelfsema, I.; Chollett, A.; Harborne, S.; Heron, S.; Weeks, W.; Skirving, A.; Strong, C.; Eakin, T.; Christensen, V.; et al. Remote sensing of coral reefs for monitoring and management: A review. *Remote Sens.* **2016**, *8*, 118. [[CrossRef](#)]
- Wilkinson, C. *Status of Coral Reefs of the World*; Australian Institute of Marine Science: Townsville, Australia, 2004; p. 301.
- Wilkinson, C. *Status of Coral Reefs of the World*; Global Coral Reef Monitoring Network and Reef and Rainforest Research Center: Townsville, Australia, 2008; p. 296.
- Gardner, T.A.; Cote, I.M.; Gill, J.A.; Grant, A.; Watkinson, A.R. Long-term region-wide declines in Caribbean corals. *Science* **2003**, *301*, 958–960. [[CrossRef](#)] [[PubMed](#)]
- Bruno, J.F.; Selig, E.R. Regional decline of coral cover in the Indo-Pacific: Timing, extent, and subregional comparisons. *PLoS ONE* **2007**, *2*, e711. [[CrossRef](#)] [[PubMed](#)]
- Jackson, J.B.C.; Donovan, M.K.; Cramer, K.L.; Lam, V.V. Status and Trends of Caribbean Coral Reefs: 1970–2012. In *Global Coral Reef Monitoring Network*; IUCN Gland: Gland, Switzerland, 2014.
- Planetary Coral Reef Foundation Overview Organization (PCRF). Mapping Coral Reefs from Space. 2002. Available online: <http://www.pcrf.org/> (accessed on 15 May 2018).
- Atkinson, J.M.; Lucey, P.G.; Taylor, G.J.; Porter, J.; Dollar, S.; Andre, S. *CRESPO: Coral Reef Ecosystem Spectro-Photometric Observatory, Concept Study Report to the University Earth System Science Program National Aeronautics and Space Administration*; University of Hawaii: Honolulu, HI, USA, 2001.
- Hochberg, E.J.; Atkinson, M.J. Capabilities of Remote Sensors to Classify Coral, Algae, and Sand as Pure and Mixed Spectra. *Remote Sens. Environ.* **2003**, *85*, 174–189. [[CrossRef](#)]
- Capolsini, P.; Andréfouët, S.; Rion, C.; Payri, C. A comparison of Landsat ETM+, SPOT HRV, IKONOS, ASTER, and airborne MASTER data for coral reef habitat mapping in South Pacific islands. *Can. J. Remote Sens.* **2007**, *29*, 187–200. [[CrossRef](#)]
- Kobryn, H.T.; Wouters, K.; Beckley, L.E.; Heege, T. Ningaloo reef: Shallow marine habitats mapped using a hyperspectral sensor. *PLoS ONE* **2013**, *8*, e70105. [[CrossRef](#)] [[PubMed](#)]
- Phinn, S.R.; Hochberg, E.; Roelfsema, C.M. Airborne photography, multispectral and hyperspectral remote sensing on coral reefs. In *Coral Reef Remote Sensing*; Goodman, J.A., Phinn, S.R., Purkis, S., Eds.; Springer: Berlin, Germany, 2013; pp. 3–25.
- Roelfsema, C.M.; Lyons, M.; Kovacs, E.M.; Maxwell, P.; Saunders, M.I.; Samper-Villarreal, J.; Phinn, S.R. Multi-temporal mapping of seagrass cover, species and biomass: A semi-automated object based image analysis approach. *Remote Sens. Environ.* **2014**, *150*, 172–187. [[CrossRef](#)]
- Hedley, J.D.; Roelfsema, C.; Brando, V.; Giardino, C.; Kutser, T.; Phinn, S.; Mumby, P.J.; Barrilero, O.; Laporte, J.; Koetz, B. Coral reef applications of Sentinel-2: Coverage, characteristics, bathymetry and benthic mapping with comparison to Landsat 8. *Remote Sens. Environ.* **2018**, *216*, 598–614. [[CrossRef](#)]

24. Traganos, D.; Aggarwal, B.; Poursanidis, D.; Topouzelis, K.; Chrysoulakis, N.; Reinartz, P. Towards Global-Scale Seagrass Mapping and Monitoring Using Sentinel-2 on Google Earth Engine: The Case Study of the Aegean and Ionian Seas. *Remote Sens.* **2018**, *10*, 1227. [CrossRef]
25. Traganos, D.; Poursanidis, D.; Aggarwal, B.; Chrysoulakis, N.; Reinartz, P. Estimating Satellite-Derived Bathymetry (SDB) with the Google Earth Engine and Sentinel-2. *Remote Sens.* **2018**, *10*, 859. [CrossRef]
26. Kutser, T.; Dekker, A.G.; Skirving, W. Modeling Spectral Discrimination of Great Barrier Reef Benthic Communities by Remote Sensing Instruments. *Limnol. Oceanogr.* **2003**, *48*, 497–510. [CrossRef]
27. Mumby, P.J.; Green, E.P.; Edwards, A.J.; Clark, C.D. The cost-effectiveness of remote sensing for tropical coastal resources assessment and management. *J. Environ. Manag.* **1999**, *55*, 157–166. [CrossRef]
28. Yamano, H. Multispectral Applications. In *Coral Reef Remote Sensing: A Guide for Multi-Level Sensing Mapping and Assessment*; Goodman, J., Purkis, S., Phinn, S.R., Eds.; Springer: Berlin, Germany, 2013; pp. 51–78.
29. El-Askary, H.; El-Mawla, S.H.A.; Li, J.; El-Hattab, M.M.; El-Raey, M. Change detection of coral reef habitat using Landsat-5 TM, Landsat 7 ETM+ and Landsat 8 OLI data in the Red Sea. *Int. J. Remote Sens.* **2014**, *35*, 2327–2346.
30. Matsunaga, T.; Hoyano, A.; Mizukami, Y. Monitoring of Coral Reefs on Ishigaki Island in Japan Using Multitemporal Remote Sensing Data. *Hyperspectral Remote Sens. Ocean* **2001**, *4154*, 212–222. [CrossRef]
31. Ahmad, W.; Neil, D.T. An Evaluation of Landsat Thematic Mapper (TM) Digital Data for Discriminating Coral Reef Zonation: Heron Reef (GBR). *Int. J. Remote Sens.* **1994**, *15*, 2583–2597. [CrossRef]
32. Jupp, D.L.B. Background and extensions to depth of penetration (DOP) mapping in shallow coastal waters. In Proceedings of the Symposium on Remote Sensing of the Coastal Zone International Symposium, Gold Coast, Queensland, Australia, 7–9 September 1988.
33. Mumby, P.J.; Skirving, W.; Strong, A.E.; Hardy, J.T.; LeDrew, E.F.; Hochberg, E.J.; Stumpf, R.P.; David, L.T. Remote Sensing of Coral Reefs and their Physical Environment. *Mar. Pollut. Bull.* **2004**, *48*, 219–228. [CrossRef] [PubMed]
34. Green, E.P.; Mumby, P.J.; Edwards, A.J.; Clark, C.D. *Remote Sensing Handbook for Tropical Coastal Management*; Edwards, A.J., Ed.; UNESCO: Paris, France, 2000.
35. Mumby, P.J.; Clark, C.D.; Green, E.P.; Edwards, A.J. Benefits of water column correction and contextual editing for mapping coral reefs. *Int. J. Remote Sens.* **1998**, *19*, 203–210. [CrossRef]
36. Cracknell, A.P.; Ibrahim, M.; McManus, J. Use of satellite and aircraft data for bathymetry studies. In Proceedings of the 13th Annual Conference of the Remote Sensing Society, Nottingham, UK, 7–11 September 1987; pp. 391–402.
37. Green, E.P.; Mumby, P.J.; Edwards, A.J.; Clark, C.D. A review of remote sensing for the assessment and management of tropical coastal resources. *Coast. Manag.* **1996**, *24*, 1–40. [CrossRef]
38. Andréfouët, S.; Hochberg, E.J.; Chevillon, C.; Muller-Karger, F.E.; Brock, J.C.; Hu, C. Multi-scale remote sensing of coral reefs. In *Remote Sensing of Coastal Aquatic Environments*; Har, R.L., Miller, X., Del Castillo, C.E., Mckee, B.A., Eds.; Springer: Dordrecht, The Netherlands, 2005; pp. 297–315.
39. Zainal, A.J.M.; Dalby, D.H.; Robinson, I.S. Monitoring of marine ecological changes on the east coast of Bahrain with Landsat TM. *Photogramm. Eng. Remote Sens.* **1993**, *59*, 415–421.
40. Bierwirth, P.N.; Lee, T.J.; Burne, R.V. Shallow sea-floor reflectance and water depth derived by unmixing multispectral imagery. *Photogramm. Eng. Remote Sens.* **1993**, *59*, 331–338.
41. Andréfouët, S.; Muller-Karger, F.E.; Hochberg, E.J.; Hu, C.; Carder, K.L. Change detection in shallow coral reef environments using Landsat 7 ETM+ data. *Remote Sens. Environ.* **2001**, *78*, 150–162. [CrossRef]
42. Andréfouët, S.; Kramer, P.; Torres-Pulliza, D.; Joyce, K.E.; Hochberg, E.J.; Garza-Perez, R.; Mumby, P.J.; Riegl, B.; Yamano, H.; White, W.H.; et al. Multi-sites evaluation of IKONOS data for classification of tropical coral reef environments. *Remote Sens. Environ.* **2003**, *88*, 128–143. [CrossRef]
43. Mumby, P.J.; Edwards, A.J. Mapping marine environments with IKONOS imagery: Enhanced spatial resolution can deliver great thematic accuracy. *Remote Sens. Environ.* **2002**, *82*, 248–257. [CrossRef]
44. Laborte, A.; Maunahan, A.; Hijmans, R. Spectral Signature Generalization and Expansion Can Improve the Accuracy of Satellite Image Classification. *PLoS ONE* **2010**, *5*, e10516. [CrossRef] [PubMed]
45. Coral Reef Ecosystem Program; Pacific Islands Fisheries Science Center. National Coral Reef Monitoring Program: Benthic Cover Derived from Analysis of Benthic Images Collected during Stratified Random Surveys (StRS) across the Pacific Remote Island Areas since 2014. NOAA's National Center for Environmental Information. 2016. Available online: <https://inport.nmfs.noaa.gov/inport/item/36157> (accessed on 15 May 2018).

46. Pacific Island Benthic Habitat Mapping Center. Palmyra Atoll. NOAA's National Center for Environmental Information. 2018. Available online: <http://www.soest.hawaii.edu/pibhmc/cms/> (accessed on 12 May 2018).
47. Palmyra Atoll National Wildlife Refuge. Ramsar Site Information Services. 2018. Available online: https://www.fws.gov/refuge/Palmyra_Atoll/ (accessed on 15 May 2018).
48. Max, L.M.; Hamilton, S.L.; Gaines, S.D.; Warner, R.R. Benthic processes and overlying fish assemblages drive the composition of benthic detritus on a central Pacific coral reef. *Mar. Ecol. Prog. Ser.* **2013**, *482*, 181–195. [[CrossRef](#)]
49. Sandin, S.A.; Smith, J.E.; DeMartini, E.E.; Dinsdale, E.A.; Donner, S.D.; Friedlander, A.M.; Konotchick, T.; Malay, M.; Maragos, J.E.; Obura, D.; et al. Baselines and degradation of coral reefs in the Northern Line Islands. *PLoS ONE* **2008**, *3*, e1548. [[CrossRef](#)] [[PubMed](#)]
50. McCauley, D.J.; Micheli, F.; Young, H.S.; Tittensor, D.P.; Brumbaugh, D.R.; Madin, E.M.P.; Holmes, K.E.; Smith, J.E.; Lotze, H.K.; DeSalles, P.A.; et al. Acute effects of removing large fish from a near-pristine coral reef. *Mar. Biol.* **2010**, *157*, 2739–2750. [[CrossRef](#)] [[PubMed](#)]
51. Knapp, I.S.; Maragos, J.E.; Vroom, P. Monitoring supports establishment of Pacific Remote Islands Marine National Monument. In Proceedings of the 12th International Coral Reef Symposium, Cairns, Australia, 9–13 July 2012.
52. Williams, G.J.; Smith, J.E.; Conklin, E.J.; Gove, J.M.; Sala, E.; Sandin, S.A. Benthic communities at two remote Pacific coral reefs: Effects of reef habitat, depth, and wave energy gradients on spatial patterns. *PeerJ* **2013**, *1*, e81. [[CrossRef](#)] [[PubMed](#)]
53. Office of Insular Affairs, Department of the Interior. *Kingman Reef*; Office of Insular Affairs, Department of the Interior: Washington, DC, USA, 2009.
54. Friedlander, A.M.; Sandin, S.A.; DeMartini, E.E. Spatial patterns of the structure of reef fish assemblages at a pristine atoll in the central Pacific. *Mar. Ecol. Prog. Ser.* **2010**, *410*, 219–231. [[CrossRef](#)]
55. Pacific Remote Islands National Wildlife Refuge Complex. *Baker Island National Wildlife Refuge: Draft Comprehensive Conservation Plan and Environmental Assessment*; Pacific Remote Islands National Wildlife Refuge Complex: Washington, DC, USA, 2007.
56. Maragos, J.; Miller, J.; Gove, J.; Mundy, B.; Friedlander, A.M.; Godwin, S.; Musburger, C.; Timmers, M.; Tsuda, R.; Vroom, P.; et al. US coral reefs in the Line and Phoenix Islands, central Pacific Ocean: History, geology, oceanography and biology. In *Coral Reefs of the USA Coral Reefs of the World 1*; Riegl, B.M., Dodge, R.E., Eds.; Springer: New York, NY, USA, 2008; pp. 595–641.
57. Miller, J.; Maragos, J.; Brainard, R.; Vroom, P.S.; Godwin, S.; Hoeke, R.K.; Aeby, G.S.; Moffitt, R.; Lammers, M.; Gove, J.; et al. The state of Coral Reef Ecosystems of the Pacific Remote Island Areas. In *The State of Coral Reef Ecosystems of the United States and Pacific Freely Associated States*; Waddell, J.E., Clarke, A.M., Eds.; NOAA Technical Memorandum NOS; NCCOS: Silver Spring, MD, USA, 2002; pp. 353–386.
58. Pacific Remote Islands National Wildlife Refuge Complex. *Howland Island National Wildlife Refuge: Draft Comprehensive Conservation Plan and Environmental Assessment*; Pacific Remote Islands National Wildlife Refuge Complex: Washington, DC, USA, 2007.
59. Edwards, A. *Applications of Satellite and Airborne Image Data to Coastal Management*; UNESCO: Paris, France, 1999.
60. Maritorena, S. Remote Sensing of the Water Attenuation in Coral Reefs: A Case Study in French Polynesia. *Int. J. Remote Sens.* **1996**, *17*, 155–166. [[CrossRef](#)]
61. Fisher, R.A. The use of multiple measurements in taxonomic problems. *Ann. Eugen.* **1936**, *7*, 179–188. [[CrossRef](#)]
62. Hastie, T.; Tibshirani, R.; Friedman, J. *The Elements of Statistical Learning: Data Mining, Inference and Prediction*, 2nd ed.; Springer: New York, NY, USA, 2009; pp. 106–111.
63. *Core Team R: A Language and Environment for Statistical Computing*; R Foundation for Statistical Computing: Vienna, Austria, 2016; Available online: <https://www.R-project.org/> (accessed on 15 May 2018).
64. Roy, D.P.; Borak, J.S.; Devadiga, S.; Wolfe, R.E.; Zheng, M.; Desclotres, J. The MODIS Land product quality assessment approach. *Remote Sens. Environ.* **2002**, *83*, 62–76. [[CrossRef](#)]
65. Ackerman, S.A.; Strabala, K.I.; Menzel, W.P.; Frey, R.A.; Moeller, C.C.; Gumley, L.E. Discriminating clear sky from clouds with MODIS. *J. Geophys. Res.* **1998**, *103*, 32141–32157. [[CrossRef](#)]
66. Chavez, P.S., Jr. An improved dark-object subtraction technique for atmospheric scattering correction for multispectral data. *Remote Sens. Environ.* **1988**, *24*, 459–479. [[CrossRef](#)]
67. Manavalan, P.; Sathyanath, P.; Rajegowda, G.L. Digital image analysis techniques to estimate waterspread for capacity evaluations of reservoirs. *Photogramm. Eng. Remote Sens.* **1993**, *59*, 1389–1395.

68. Gitelson, A.A.; Ya Kondratyev, K. Optical models of mesotrophic and eutrophic water bodies. *Int. J. Remote Sens.* **1991**, *12*, 373–385. [[CrossRef](#)]
69. Chavez, P.S., Jr. Image-Based Atmospheric Corrections—Revisited and Improved. *Photogramm. Eng. Remote Sens.* **1996**, *62*, 1025–1036.
70. Tassan, S. Modified Lyzenga’s method for macroalgae detection in water with non-uniform composition. *Int. J. Remote Sens.* **1996**, *17*, 1601–1607. [[CrossRef](#)]
71. Gordon, H.R.; Morel, A. *Remote Assessment of Ocean Color for Interpretation of Satellite Visible Imagery*; Springer: New York, NY, USA, 1983.
72. Vanderstraete, T.; Goossens, R.; Ghabour, T.K. Coral Reef Habitat Mapping in The Red Sea (Hurghada, Egypt) Based on Remote Sensing. *EARSeL eProc.* **2004**, *3*, 191–207.
73. Armstrong, R.A. Remote sensing of submerged vegetation canopies for biomass estimation. *Int. J. Remote Sens.* **1993**, *14*, 621–627. [[CrossRef](#)]
74. Lyzenga, D. Remote Sensing of Bottom Reflectance and Water Attenuation Parameters in Shallow Water Using Aircraft and Landsat Data. *Int. J. Remote Sens.* **1981**, *2*, 71–82. [[CrossRef](#)]
75. Lyzenga, D. Passive remote sensing techniques for mapping water depth and bottom features. *Appl. Opt.* **1978**, *17*, 379–383. [[CrossRef](#)] [[PubMed](#)]
76. Paredes, J.M.; Spero, R.E. Water depth mapping from passive remote sensing data under a generalized ratio assumption. *Appl. Opt.* **1983**, *22*, 1134–1135. [[CrossRef](#)] [[PubMed](#)]
77. Gould, R.W.; Arnone, R.A., Jr.; Sydor, M. Absorption, Scattering, and Remote Sensing Reflectance Relationships in Coastal Waters: Testing a New Inversion Algorithm. *J. Coast. Res.* **2001**, *17*, 328–341.
78. Le, J.A.; El-Askary, H.M.; Allali, M.; Struppa, D.C. Application of recurrent neural networks for drought projections in California. *Atmos. Res.* **2017**, *188*, 100–106. [[CrossRef](#)]



© 2018 by the authors. Licensee MDPI, Basel, Switzerland. This article is an open access article distributed under the terms and conditions of the Creative Commons Attribution (CC BY) license (<http://creativecommons.org/licenses/by/4.0/>).